

# 1 The generation of crystal-poor rhyolite in the upper crust

2 Eva Hartung, Luca Caricchi

3 Department of Earth Sciences, University of Geneva, Rue des Maraîchers 13, 1205 Geneva,

4 Switzerland

5

6 Corresponding authors:

7 Eva Hartung email: [eva.hartung@unige.ch](mailto:eva.hartung@unige.ch)

8

9 Keywords: rhyolite-MELTS, silicic volcanism, water content, melt extraction, hindered settling,

10 physical properties, Takidani pluton

11

## 12 **ABSTRACT**

13 The extraction of felsic melts, from crystallizing crustal magma reservoirs, is essential for the

14 chemical evolution of the crust and is a phenomenon preceding some of the largest eruptions on

15 Earth. The physical properties of residual melt and magma and the time at which the conditions

16 remain appropriate for melt extraction are the most important factors controlling the efficiency of

17 melt extraction and the distribution of melt in magma reservoirs. We use rhyolite-MELTS

18 simulations to evaluate the physical evolution of crystallizing granodioritic (or dacitic) hydrous

19 magma (i.e.  $\geq 1$  wt.% H<sub>2</sub>O) at 200 MPa. These results allow us to estimate extraction velocities of

20 residual melt and to identify the optimal conditions at which melt segregation occurs. We

21 additionally estimate the time that magma reservoirs of different thicknesses spend within the

22 window that is best suited for magma extraction. Hydrous magmas that attain water saturation

23 after 40 wt.% crystallization (rheological locking point) are best suited for melt extraction. In

24 fact, once water-saturation is achieved, the rate of release of latent heat of crystallization  
25 increases while the viscosity of the residual liquid and crystal-liquid density contrast remain  
26 favorable for melt segregation. We test our findings on the Takidani pluton (Japan) because it  
27 shows clear evidences of residual melt segregation from crystallizing magma, and was associated  
28 with caldera-forming eruptions. In agreement with geochemistry, the calculations show that most  
29 of the melt-rich body at the top of the pluton was formed once the pluton crystallized to 40-50  
30 wt.% and water-saturation was achieved. Estimates of the duration of cooling in this system  
31 suggest that residual melt properties were appropriate to allow the formation of a single melt-rich  
32 lens at the top of the reservoir. Our results can be generalized to upper crustal magma reservoirs  
33 and suggest that sufficiently large upper crustal reservoirs containing granodioritic (i.e. dacitic)  
34 magma with more than 3 wt.% H<sub>2</sub>O can produce large melt-rich caps at the top of partially  
35 crystallized magma within relatively short timescales. In H<sub>2</sub>O-poorer magmas the time available  
36 for melt extraction is not sufficient for complete extraction of the residual melt, which, therefore,  
37 accumulates in isolated pockets. The tendency of water-poorer magmas to form melt-rich lenses  
38 within partially crystallized magma may decrease our capacity of detecting eruptible magma  
39 using geophysical methods in volcanic systems such as Yellowstone.

40

## 41 **1. Introduction**

### 42 *1.1. Crystal-liquid separation in the upper crust*

43 Segregation of interstitial melt from a rheologically-locked partially-crystallized magma has  
44 been proposed by various authors as a potential mechanism for the generation of shallow and  
45 voluminous reservoirs of crystal-poor and eruptible rhyolite (Bachmann and Bergantz, 2004;  
46 Dufek and Bachmann, 2010; Hildreth, 2004, 1981; Hildreth and Wilson, 2007; Marsh, 1981).

47 Thermo-mechanical simulations suggest that the efficiency of melt extraction for common  
48 hydrous silicic magma compositions is highest at crystal contents between 50% and 70% (Dufek  
49 and Bachmann, 2010). These studies also emphasize that the probability for interstitial melt  
50 extraction is not only controlled by the physical properties of residual melt and magma, but by  
51 the time spent by magma at conditions best suited for melt extraction (Dufek and Bachmann,  
52 2010; Huber et al., 2009). This, in turn, is function of the topology of the phase diagram,  
53 specifically of the rate of latent heat release during progressive cooling, and evolution of the  
54 physical properties of the residual melt of magma with increasing crystallinity (Caricchi and  
55 Blundy, 2015; Huber et al., 2009; Lee et al., 2015; Melekhova et al., 2013). The results of these  
56 studies permit to draw some general conclusions about extraction of residual melt in felsic  
57 systems: i) Independently of the process leading to the extraction of residual melt in crystallizing  
58 felsic magmas, the separation between residual melt and crystals occurs when magma is  
59 rheologically locked (i.e. crystal fraction  $>0.4$ ; Dufek and Bachmann, 2010; Huber et al., 2010;  
60 Marsh, 1981; Pistone et al., 2015); ii) The velocity of residual melt extraction is directly  
61 proportional to the ratio between the density difference of crystals and residual melt and the  
62 viscosity of the residual melt (Bachmann and Bergantz, 2004; Dufek and Bachmann, 2010) ; iii)  
63 The longer magma spends at conditions suitable for residual melt extraction, the larger is the  
64 amount of residual melt extracted (Dufek and Bachmann, 2010; Huber et al., 2009).

65 Evidences for large-scale segregation of rhyolitic melts is commonly retrieved from  
66 volcanic sequences (Bachmann and Bergantz, 2004; Deering et al., 2011; Hildreth and Wilson,  
67 2007), however, such testimony is scarce or obscure in the intrusive record (Coleman et al.,  
68 2004; Gelman et al., 2014; Vigneresse, 2014). The Takidani pluton is texturally zoned, with a  
69 gradual transition (over about 50 m) from equigranular to porphyritic texture (Fig. 1). The whole

70 rock chemistry of the equigranular (GDT) and the porphyritic portions (pGT) of the intrusion,  
71 suggest that pGT was extracted from GDT once the residual melt fraction dropped to 40-50 wt.%  
72 (Figs. 1, 2a; Hartung et al., 2017). These findings are confirmed by trace element analyses  
73 carried out on plagioclase (Fig. 2b). Additionally, the composition, mineral chemistry and age, of  
74 the Takidani pluton and volcanic products distributed across Japan are similar, which supports  
75 the hypothesis that the Takidani pluton fed volcanic activity (Kataoka et al., 2001; Kimura and  
76 Nagahashi, 2007). This makes the Takidani pluton an excellent candidate to investigate the  
77 formation of shallow rhyolitic reservoirs and the build-up to large caldera-forming eruptions. In  
78 this study, we calculate the variation of the physical properties of magma and residual melt for  
79 granodioritic (i.e. dacitic) magmas that are comparable to those of the Takidani pluton, for a  
80 range of initial water contents ( $H_2O_i$ ) between 1 and 6 wt.%. We aim 1) to constrain the effect of  
81  $H_2O_i$  content on the efficiency of melt extraction, 2) to identify the conditions that led to the  
82 extraction of residual melt from the Takidani pluton, and 3) to define the impact of  $H_2O_i$  content  
83 on the architecture of upper crustal magma reservoirs.

84

## 85 **2. Material and methods**

### 86 *2.1. Rhyolite-MELTS*

87 Existing experimental data do not cover the entire range of temperature and water content  
88 required to trace the evolution of residual melt during cooling and crystallization of magma in  
89 the upper crust (Costa et al., 2004; Holtz et al., 2005; Scaillet and Evans, 1999). Thus, we use  
90 rhyolite-MELTS (Gualda et al., 2012) to calculate the chemical and physical evolution of  
91 residual melt of granodioritic magma from liquidus to solidus temperature and over the entire  
92 range of initial water content between 1 and 6 wt.%. Because granodiorites represent about 95

93 wt.% of the upper crust (Rudnick and Gao, 2003) and because the main portion of the Takidani  
94 pluton is granodioritic with a composition similar to the starting material of Costa et al. (2004;  
95 Hartung et al., 2017), we use this composition for the rhyolite-MELTS calculations. This  
96 composition also allows us to test the performance of rhyolite-MELTS, especially in reproducing  
97 the residual melt compositions produced experimentally by Costa et al. (2004).

98         In our rhyolite-MELTS simulations we force crystallization by removing an equal  
99 amount of heat from the system (i.e. 1 J/g) at each step ( $n$ ) starting from the liquidus temperature  
100 down to a temperature ( $T$ ) of about 740°C, which corresponds to a residual melt fraction of about  
101 0.1. With this approach, we assume that a fix rate of heat is being released from the magma (i.e.  
102 constant heat loss). Thus, the number of modeling steps within a given temperature interval  
103 becomes proportional to the time spent by the magma within that interval of temperature. This is  
104 important to be able to quantify the total time that magma spends within the temperature and  
105 crystallinity range at which residual melt extraction occurs (Dufek and Bachmann, 2010).

106         For all calculations, the confining pressure was fixed at 200 MPa, which are the  
107 conditions applied in the Costa et al. (2004) experiments and are close to the inferred  
108 emplacement depth for the Takidani pluton (Hartung et al., 2017). The oxygen fugacity was  
109 initially fixed to the nickel-nickel oxide buffer (NNO) to calculate the liquidus temperature (for  
110 different  $H_2O_i$ ), but remained unconstrained during progressive heat extraction. Although  
111 rhyolite-MELTS does not capture all subtleties of the phase equilibria for hydrous magmas (i.e.  
112 amphibole and biotite crystallization), the residual melt composition varies as function of  
113 temperature and water content following the experimental residual liquids of the experiments of  
114 Costa et al. (2004; Fig.3).

115

116        *2.2. The Takidani pluton: evidences of melt segregation and eruption*

117 In the following we provide a summary of the main results of a geochemical study previously  
118 performed on the Takidani pluton (Hartung et al., 2017). The Takidani pluton is a well exposed  
119 and extremely young pluton (1.63 Ma, Ito et al., 2017), located in the Central Japan Alps and it is  
120 thought to present the source of voluminous dacitic and rhyolitic eruptions at the Plio-  
121 Pleistocene boundary (Kimura and Nagahashi, 2007). The pluton is vertically exposed over 1800  
122 m (Fig. 1; Harayama et al., 2003) from a tectonic contact at the base to a magmatic roof contact  
123 with older volcanic lithology (i.e. Hotaka Andesite, Harayama, 1994). Textural, chemical and  
124 isotopic evidence of large-scale melt segregation is observed in the upper part of the pluton  
125 (Figs. 1,2; Hartung et al., 2017). The rock textures of the Takidani pluton change from  
126 holocrystalline to progressively more porphyritic appearance from the base and center to the roof  
127 of the intrusion. Major and trace element whole rock analysis and data obtained through  
128 quantitative evaluation of minerals by QEMSCAN and electron microprobe analyses (EMPA)  
129 are used to determine the area percent and chemical composition of the matrix components  
130 (equivalent to residual melt composition) throughout the upper section of the Takidani pluton  
131 (Fig. 1). This data shows a progressive increase in the residual melt components defined by  
132 quartz (Qtz), alkali feldspar (Kspar) and albite-rich plagioclase (Plg<An30) from the  
133 equigranular granodiorite (GDT) to the porphyritic granite (pGT; Fig. 1). However, the relative  
134 fraction of quartz (Qtz), albite (Ab), and orthoclase (Or) and therefore the melt compositions  
135 remains constant across the textural and chemical transition and suggest that the residual melt  
136 had a chemical composition equivalent to the granitic minimum at approximately 200 MPa  
137 (Johannes and Holtz, 1996).

138 Hartung et al. (2017) show that magmatic differentiation in the Takidani pluton is dominated  
139 by crystal fractionation with minor assimilation of older partially molten granite (Fig. 2a).  
140 Concentrations of Rb in plagioclase increases from core to rim and can be modeled with the  
141 crystallization of magma to more than 50 wt.% (Fig. 2b). All plagioclases are characterized by a  
142 common rim, which formed when the magma crystal fraction reached 40-50 wt.%. The  
143 ubiquitous presence of such plagioclase rims indicates that the magma reached its rheological  
144 locking point at this crystallinity (Fig. 2b). Additionally, petrographic observations suggest that  
145 plagioclase started crystallizing at temperatures of about 900-850°C and before amphibole  
146 reached its liquidus temperature (~850°C). The distribution of temperature estimates in  
147 amphibole and comparison to phase equilibria experiments from Costa et al. (2004) highlight  
148 that amphibole dominantly grew under low temperature conditions (<800°C, Hartung et al.,  
149 2017) and crystallinities of >40 wt.%, which again corresponds to the rheological locking of  
150 crystal mushes (Caricchi et al., 2007; Pistone et al., 2013). The late appearance of amphibole  
151 thus not only indicates emplacement and crystallization at pressure of about 200 MPa, but that  
152 the initial water content of the granodioritic magma was between 3 and 4 wt.% and that the  
153 extraction of residual melt from the crystallizing magma occurred under water saturated  
154 conditions (Costa et al., 2004; Hartung et al., 2017). These evidences show that the pGT unit  
155 represents a lens of residual melt extracted from the underlying GDT granodiorite.

156

### 157 **3. Results**

#### 158 *3.1. Thermal, chemical and physical evolution of dacitic magma*

159 Water has an important effect on phase equilibria as it depresses liquidus temperatures and  
160 modifies the relationships between crystallinity, physical properties of magmas and temperature

161 (e.g. viscosity and density of the residual melt ; Caricchi et al., 2007; Giordano et al., 2008;  
162 Lange, 1994; Melekhova et al., 2013; Whitney, 1988). The extraction of heat from a magma  
163 reservoir forces its crystallization and causes silica and water enrichment in the residual melt  
164 (Fig. 4). Once the residual melt becomes water saturated,  $H_2O_i$ -undersaturated magmas join the  
165  $T$ -crystallinity trajectory of  $H_2O_i$ -saturated magma (Fig. 4). At 200 MPa the liquidus temperature  
166 of granodioritic (or dacitic) magma with an initial water content of 1 wt.% lies at 1080°C  
167 (rhyolite-MELTS), while the liquidus temperature of water saturated (about 6 wt%  $H_2O$ ; Ghiorso  
168 and Gualda, 2015) dacitic magma is 110°C lower (Fig. 5a). Such difference in liquidus  
169 temperature implies that relatively drier magmas have a higher initial heat content with respect to  
170 water-bearing magmas, thus, leading to longer cooling periods. Moreover, the initial water  
171 content affects the relationship between temperature and crystallinity of magma (Fig. 5a;  
172 Whitney, 1988). The rate of crystallization is non-linear for hydrous magmas. Thus, the rate of  
173 latent heat release is not constant and in a system in which heat is extracted at approximately  
174 constant rate, magma spends the largest amount of time at temperatures where the rate  
175 crystallization (i.e. rate of latent heat release) is highest (Caricchi and Blundy, 2015; Marsh,  
176 1981). Water also affects the evolution of density contrast between crystals and residual melt and  
177 the viscosity of the residual melt within the rheologically locked region, which, in turn,  
178 modulates the velocity of residual melt extraction (Figs. 5b, c; Bachman and Bergantz, 2004).  
179 Regardless of the initial water content of the magma, residual melt viscosity increases down to  
180 melt fractions of 0.5-0.4 because of decreasing temperature and increasing silica content. At  
181 lower melt fractions (<0.4) and once volatile saturation is achieved, the viscosity of the residual  
182 melt remains unchanged independent of the initial water content (Fig. 5b). Relatively dry melts  
183 ( $H_2O_i \leq 2$  wt.%) reach a maximum in viscosity before joining the viscosity-temperature path at



184 low melt fractions (Fig. 5b). The contrast in density between the solid phase and residual melt  
185 spans a wide range of values at near liquidus conditions (for different  $H_2O_i$ ) but becomes less  
186 dependent on  $H_2O_i$  for melt fractions  $<0.6$  (Fig. 5c). The ratio of the difference in density  
187 between crystals and residual melt and the viscosity of the residual melt, which is directly related  
188 to the velocity of melt extraction (Bachman and Bergantz, 2004), generally increases with water  
189 content (Figs. 5b, c).

190         Based on the above and when considering only the physical properties of the residual  
191 melt, the extraction velocity of residual melt is the fastest for  $H_2O_i$ -saturated magmas. However,  
192 the total time spent by magma at melt fractions  $<0.6$  (i.e. rheologically locked conditions) is  
193 inversely proportional to the initial water content of magma (Fig. 5d). To assess the relative  
194 importance of the initial water content on the physical properties of magma and the timescales  
195 available for melt segregation to occur, we calculate the velocity of melt extraction by hindered  
196 settling for granodioritic-dacitic magma throughout the rheologically locked portion of the  
197 magmatic cooling history (melt fraction  $<0.6$ ). We notice that the process of residual melt  
198 extraction in this formulation is simplified but we are interested in the comparison between the  
199 efficiency of residual melt for magmas with different initial water contents. Compaction or gas-  
200 filter pressing are viable mechanisms but an accurate analysis of the mechanisms responsible for  
201 the extraction of residual melt is beyond the scope of this contribution.

202

### 203         3.2. *Timescales of melt segregation*

204 We use the physical properties obtained from rhyolite-MELTS simulations to calculate hindered  
205 settling velocities ( $U_{hs}$ ) for crystallizing magma reservoirs (i.e. Takidani pluton) following the  
206 equation provided by Bachmann and Bergantz (2004):

207

$$208 \quad U_{hs} = \frac{2r^2 g \Delta\rho r}{9\mu} \frac{(1-c)^2}{(1+c^{1/3})^{[5c/3(1-c)]}} \quad (1)$$

209

210 Where  $r$  is the crystal radius,  $g$  is gravitational acceleration ( $9.81 \text{ ms}^{-1}$ ),  $\Delta\rho$  is the density  
211 difference between crystal and melt,  $\mu$  is the viscosity of the melt and  $c$  is the crystal fraction.  
212 Crystal fraction and size control porosity and permeability of silicic mushes (McKenzie, 1984),  
213 and can affect melt extraction velocity by several orders of magnitude (Bachmann and Bergantz,  
214 2004). To compare the velocities obtained for magmas with different  $H_2O_i$ , we always consider a  
215 crystal radius of 3 mm, which is appropriate for the Takidani pluton (Fig. 1; Hartung et al.,  
216 2017). Settling velocities vary between 3.0 and 0.02 m/yr for melt fractions decreasing from 0.6  
217 to 0.2 (Fig. 6). Segregation velocities for  $H_2O_i \geq 3$  wt.%, i.e. within the rheologically locked  
218 interval remain essentially the same because the residual melt at these crystallinities is water  
219 saturated (Fig. 6). Magmas with  $H_2O_i < 3$  wt.%, however, become water saturated at lower  
220 temperature and at higher crystallinities resulting in much slower settling velocities mainly  
221 because of their higher viscosity. Based on these calculations, the residual melt separates more  
222 efficiently from highly crystallized dacitic magmas if the initial water concentration is equal or  
223 greater than 3 wt.%. It is important to stress that these conclusions are valid for a confining  
224 pressure of 200 MPa. Water solubility in magma increases with pressure, thus, at higher pressure  
225 the threshold of  $H_2O_i$  at which the increase of segregation efficiency occurs is higher.

226 The relative amount of melt that can be extracted depends on the period of time that  
227 magma spends within the rheologically locked temperature interval, which, in turn, is function of  
228 magma temperature and the crystallization rate (i.e. rate of release of latent heat of

229 crystallization) within the rheologically locked interval. For  $H_2O_i \leq 3$  wt.% the average magma  
230 temperature within the rheologically locked interval increases (Fig. 5a). When  $H_2O_i$ -  
231 undersaturated magmas reach volatile saturation, the rate of crystallization sharply increases  
232 resulting in an increase of the rate of release of latent heat of crystallization (Fig. 5a; Marsh,  
233 1981, Caricchi and Blundy, 2015b). Magmas that formed the Takidani pluton were initially  $H_2O$ -  
234 undersaturated with water contents of about 3 to 4 wt.% (Hartung et al., 2017; Costa et al.,  
235 2004). The residual melt would have reached volatile saturation at melt fractions of about 0.70 to  
236 0.55 and temperatures around 820°C to 780°C (Fig. 5a,b), at which point an increase of  
237 crystallization rate, enhanced release of latent heat of crystallization, and decreased magma  
238 cooling rates are expected. This is confirmed by amphibole thermometry, as the largest number  
239 of amphiboles measured in the granodiorite portion of the Takidani intrusion suggest prolonged  
240 residence within a relatively narrow temperature interval below 800°C (Hartung et al., 2017).

241 Our rhyolite-MELTS calculations and experimental phase relationships (Costa et al.,  
242 2004) indicate that the Takidani pluton initially contained about 3 to 4 wt.%  $H_2O$  and spent a  
243 relatively large fraction of its cooling timescale at melt fractions  $<0.65$  (Fig. 5d). The interplay  
244 between the viscosity of the residual melt, the density contrast between residual melt and  
245 crystals, and the time spent within the rheologically locked crystallinity interval, favored the  
246 extraction of residual melt from the Takidani pluton (Fig. 5).

247 In the following we investigate how the initial amount of water dissolved in magma can  
248 affect the architecture of partially crystallized dacitic reservoirs. More specifically we calculate  
249 the potential for the formation of melt-rich rhyolitic lenses within partially crystallized magma,  
250 or caps at the roof of magma reservoirs (Bachmann and Bergantz, 2004; Wotzlaw et al., 2014).

251

252 **4. Discussion**

253 4.1. *Application to the Takidani pluton*

254 We estimate the time required for magma to cool to a crystal fraction of 0.1 by 1) considering the  
255 total enthalpy content (from rhyolite-MELTS) of a magmatic reservoir constituted of fully  
256 molten granodioritic magma and 2) removing heat by applying a constant heat loss per surface  
257 area. For a fixed volume, reservoirs with high aspect ratios (i.e. diameter to thickness ratio) have  
258 larger surface area and, thus, cool faster. The time available for melt migration is equal to the  
259 time the magma spends within the rheologically locked temperature range. The distance travel by  
260 the melt is the cumulative sum of the hindered settling velocity calculated for each temperature  
261 range, multiplied by the time the magma spends within each temperature range.

262 For the Takidani Pluton, we consider a cylindrical shape and a volume of 80 km<sup>3</sup> with a  
263 radius of 6.5 km (i.e. 13 km length; Harayama, 1992) and mush thickness of 0.6 km (i.e. GDT  
264 and pGT units, Hartung et al. 2017). These are the dimensions of the exposed portion of the  
265 pluton and are therefore minimum reservoir volume estimates. The observed column of extracted  
266 melt (h) corresponds to the pGT unit in the upper part of the pluton (270 m; Fig. 1, Hartung et al.  
267 2017). The total amount of enthalpy available for the Takidani reservoir for a dacitic  
268 composition, a fixed bulk density of 2500 kg/m<sup>3</sup> and initial water content of 3 and 4 wt.% is 3.1  
269 and 2.8 x 10<sup>19</sup> J, respectively. To estimate the cooling timescale from the liquidus to a  
270 temperature corresponding to a melt fraction of 0.1, we use a constant heat loss of 2 J/s/m<sup>2</sup>,  
271 which is comparable to average heat flow measurements at Yellowstone Caldera (DeNosaquo et  
272 al., 2009). Cooling from liquidus to a melt fraction of 0.1 for such reservoir geometry, would  
273 have been completed in 1500-1700 years for magmas with initial water contents of 4 to 3 wt.%,  
274 respectively. We normalize these cooling timescales to the number of simulation steps from

275 rhyolite-MELTS to calculate the time magma spent within each simulation step. By multiplying  
276 the time within each step by the corresponding hindered settling velocity for the corresponding  
277 temperature (Fig. 6), we calculate the distance travel by the melt while the magma was in a  
278 rheologically locked state (i.e. 0.6-0.2 melt fraction). Rhyolite-MELTS simulations in  
279 combination with our estimates of cooling timescales show that the segregation of the 270 m  
280 pGT unit occurred over 220 -160 years. Such timescales indicate that the extraction of residual  
281 melt is a relatively fast process that currently cannot be resolved with geochronology (e.g.  
282 Wotzlaw et al., 2014). Using the approach applied to the Takidani pluton, in the following we  
283 estimate the potential amount of residual melt extracted from magma reservoirs of different  
284 volumes containing dacitic magma with different initial H<sub>2</sub>O content (1-6 wt.%).

285

#### 286 *4.2. The control of H<sub>2</sub>O<sub>i</sub> on the extraction of residual melt from crystallizing magmas*

287 Geochemical and petrologic studies show that crystal poor rhyolites are sourced either from caps  
288 at the top of partially crystallized reservoirs (Bachmann and Bergantz, 2004; Hildreth and  
289 Wilson, 2007), or from the amalgamation of isolated melt pockets dispersed within a highly  
290 crystallized magma (Wotzlaw et al., 2014, Ellis et al., 2014). However, the processes responsible  
291 for the generation of reservoirs with such distinct architecture are not yet fully understood.  
292 Considering the extraction of residual melt by any physical process, the final distribution of  
293 crystal-poor melt will be determined by the total distance the melt can travel before the system  
294 cools to its solidus temperature. Thermally, the maximum amount of crystal-poor melt that can  
295 potentially be accumulated depends mainly on the mass of magma within a magmatic system  
296 (i.e. heat content) and on its volume to surface ratio (rate of heat loss; Fig. 7). Our results show  
297 that chemically, the initial amount of water dissolved in dacitic magmas affects both the total

298 amount of time magmas spend within the rheologically locked temperature interval and the  
299 velocity of residual melt extraction from crystallizing magmas (Figs. 5d, 6, 7). To identify which  
300 magma compositions are best suited for the formation of melt caps or lenses, we first calculate  
301 the cooling timescale by considering a constant heat loss of  $2 \text{ J/s/m}^2$  for dacitic magmas with  
302 different  $H_2O_i$  for reservoirs of different volume and aspect ratio volumes (volume =  $10^2$ - $10^4 \text{ km}^3$   
303 and thicknesses 1-5 km). We assume that a melt-rich cap forms at the top of the reservoir if  
304 segregation velocities and time within the rheologically locked temperature window are  
305 sufficiently high for the residual melt to reach the top of the reservoir before the magma reaches  
306 a crystal fraction of 0.8. Hence, to extract fifty percent of residual melt, the calculated  
307 segregation distance needs to be half of the thickness of the magma reservoir. If less melt is  
308 extracted the residual melt needs to travel further. If velocities are lower or if reservoir aspect  
309 ratios are low (i.e. horizontally extended reservoirs), the melt does not reach the roof of the  
310 magma reservoir before cooling to 80 wt.% crystals. In this case we consider that isolated melt-  
311 rich pockets form within a highly crystallized magma.

312 Our calculations show that the residual melt of magmas containing more than 3 wt.%  $H_2O_i$   
313 moves greater distances in shorter timescales (Fig. 7) and are very likely to form crystal rich caps  
314 at or near the roof of the magma reservoir (Fig. 8). Magmas with less than 2 wt.%  $H_2O_i$  are  
315 unlikely to form any melt-rich body independent of the size or thickness of the magma reservoir  
316 (Figs. 7,8). Although magmas with 1 wt.%  $H_2O_i$  spent half of their cooling time within the  
317 rheological locking temperature window, because of the high viscosity of the residual melt (i.e.  
318 low extraction velocity) they tend not to form caps or melt-rich lenses of crystal poor rhyolite.

319

## 320 **5. Conclusions**

321 The Takidani magmatic reservoir formed, what appears to be, a cap of segregated residual melt  
322 near the roof of the magmatic reservoir (Hartung et al., 2017). With an estimated initial water  
323 content of 3-4 wt.% and a thickness of 0.6 km, segregation of the residual melt to form the 270m  
324 thick pGT unit would have occurred between 220 and 160 years. The fact, that the Takidani  
325 pluton shows evidence of large-scale melt segregation may be associated with its water  
326 undersaturation at time of emplacement, which prolonged the time spent within the rheologically  
327 locked temperature range (Fig. 5d).

328  $H_2O_i$  appears to have a pronounced impact on the potential of formation of crystal-poor melt  
329 caps or separate melt pockets. Dacitic magma mushes with  $H_2O_i \geq 3$  wt.% are most likely to form  
330 large melt caps at the roof of a magma reservoir, while magmas with  $H_2O_i < 3$  wt.% tends to form  
331 separate melt pockets due to slower segregation velocities. Magmas with  $H_2O_i \ll 2$  wt.% are  
332 unlikely to show any signs of segregation of rhyolitic melts (Fig. 7).

333 Our calculations support the hypothesis that the porphyritic unit observed at the roof of the  
334 Takidani Pluton presents a melt-rich cap. Considering a thicker or more volumetric magma  
335 reservoir would strengthen this conclusion (Fig. 8). Our simplified model only considers constant  
336 heat diffusion across a fixed magma surface, however, it captures the fundamental parameters  
337 controlling the architecture of upper crustal magma reservoirs. The initial magma water content  
338 has a significant control on the potential of magma reservoir to form melt-rich caps or isolated  
339 melt pockets dispersed in a highly-crystallized magma. Our calculations suggest that while water  
340 rich magmas have the highest potential to form melt-rich caps, water poorer magma, as those  
341 typical of the Snake River Plane (USA), should have a higher tendency to form dispersed melt-  
342 rich lenses within magma mushes. This is in agreement with geochemical data, suggesting that  
343 eruptions in the Snake River Plane are fed by multiple melt-rich lenses (Wotzlaw et al., 2014,

344 Ellis et al., 2014) and suggests that detection of eruptible magmas using geophysical methods,  
345 may be more complicated in H<sub>2</sub>O-poor systems.

346

## 347 **6. Acknowledgements**

348 This work was supported by the Swiss National Fund [SNSF grant 200021\_150204].

349

## 350 **7. References**

351 Bachmann, O., Bergantz, G., 2004. On the Origin of Crystal-poor Rhyolites : Extracted from  
352 Batholithic Crystal Mushes. *J. Petrol.* 45, 1565–1582. doi:10.1093/petrology/egh019

353 Caricchi, L., Blundy, J., 2015. Experimental petrology of monotonous intermediate magmas.  
354 *Geol. Soc. London, Spec. Publ.* doi:10.1144/SP422.9

355 Caricchi, L., BURLINI, L., ULMER, P., GERYA, T., VASSALLI, M., PAPALE, P., 2007. Non-  
356 Newtonian rheology of crystal-bearing magmas and implications for magma ascent  
357 dynamics. *Earth Planet. Sci. Lett.* 264, 402–419. doi:10.1016/j.epsl.2007.09.032

358 Coleman, D.S., Gray, W., Glazner, A.F., 2004. Rethinking the emplacement and evolution of  
359 zoned plutons: Geochronologic evidence for incremental assembly of the Tuolumne  
360 Intrusive Suite, California. *Geology* 32, 433–436. doi:10.1130/G20220.1

361 Costa, F., Scaillet, B., Pichavant, M., 2004. Petrological and Experimental Constraints on the  
362 Pre-eruption Conditions of Holocene Dacite from Volcan San Pedro (36°S, Chilean Andes)  
363 and the Importance of Sulphur in Silicic Subduction-related Magmas. *J. Petrol.* 45, 855–  
364 881. doi:10.1093/petrology/egg114

365 Deering, C.D., Cole, J.W., Vogel, T.A., 2011. Extraction of crystal-poor rhyolite from a  
366 hornblende-bearing intermediate mush: A case study of the caldera-forming Matahina



367 eruption, Okataina volcanic complex. *Contrib. to Mineral. Petrol.* 161. doi:10.1007/s00410-  
368 010-0524-0

369 DeNosaquo, K.R., Smith, R.B., Lowry, A.R., 2009. Density and lithospheric strength models of  
370 the Yellowstone–Snake River Plain volcanic system from gravity and heat flow data. *J.*  
371 *Volcanol. Geotherm. Res.* 188, 108–127. doi:10.1016/J.JVOLGEORES.2009.08.006

372 Dufek, J., Bachmann, O., 2010. Quantum magmatism: Magmatic compositional gaps generated  
373 by melt-crystal dynamics. *Geology* 38, 687–690. doi:10.1130/G30831.1

374 Ellis, B.S., Bachmann, O., Wolff, J. a., 2014. Cumulate fragments in silicic ignimbrites: The case  
375 of the Snake River Plain. *Geology* 42, 431–434. doi:10.1130/G35399.1

376 Gelman, S.E., Deering, C.D., Bachmann, O., Huber, C., Gutiérrez, F.J., 2014. Identifying the  
377 crystal graveyards remaining after large silicic eruptions. *Earth Planet. Sci. Lett.* 403, 299–  
378 306. doi:10.1016/j.epsl.2014.07.005

379 Ghiorso, M.S., Gualda, G. a. R., 2015. An H<sub>2</sub>O–CO<sub>2</sub> mixed fluid saturation model compatible  
380 with rhyolite-MELTS. *Contrib. to Mineral. Petrol.* 169, 53. doi:10.1007/s00410-015-1141-8

381 Giordano, D., Russell, J.K., Dingwell, D.B., 2008. Viscosity of magmatic liquids: A model.  
382 *Earth Planet. Sci. Lett.* 271, 123–134. doi:10.1016/j.epsl.2008.03.038

383 Gualda, G.A.R., Ghiorso, M.S., Lemons, R. V., Carley, T.L., 2012. Rhyolite-MELTS: a  
384 Modified Calibration of MELTS Optimized for Silica-rich, Fluid-bearing Magmatic  
385 Systems. *J. Petrol.* 53, 875–890. doi:10.1093/petrology/egr080

386 Harayama, S., 1994. Cooling History of the youngest exposed pluton in the World - The Plio-  
387 Pleistocene Takidani Granodiorite (Japan Alps, central Japan). *Mem. Geol. Soc. Japan* 43,  
388 87–97.

389 Harayama, S., Wada, H., Yamaguchi, Y., 2003. Trip A1 Quaternary and Pliocene granites in the

390 Northern Japan Alps. Hutt. Symp. V, F. Guideb.

391 Hartung, E., Caricchi, L., Floess, D., Wallis, S., Harayama, S., Kouzmanov, K., Chiaradia, M.,  
392 2017. Evidence for residual melt extraction in the Takidani Pluton, Central Japan. *J. Petrol.*  
393 58, 763–788. doi:10.1093/petrology/egx033

394 Hildreth, W., 2004. Volcanological perspectives on Long Valley , Mammoth Mountain , and  
395 Mono Craters : several contiguous but discrete systems. *J. Volcanol. Geotherm. Res.* 136,  
396 169–198. doi:10.1016/j.jvolgeores.2004.05.019

397 Hildreth, W., 1981. Gradients in silicic magma chambers: Implications for lithospheric  
398 magmatism. *J. Geophys. Res. Solid Earth* 86, 10153–10192. doi:10.1029/JB086iB11p10153

399 Hildreth, W., Wilson, C.J.N., 2007. Compositional Zoning of the Bishop Tuff. *J. Petrol.* 48, 951–  
400 999. doi:10.1093/petrology/egm007

401 Holtz, F., Sato, H., Lewis, J., Behrens, H., Nakada, S., 2005. Experimental petrology of the  
402 1991-1995 Unzen dacite, Japan. Part I: Phase relations, phase composition and pre-eruptive  
403 conditions. *J. Petrol.* 46, 319–337. doi:10.1093/petrology/egh077

404 Huber, C., Bachmann, O., Dufek, J., 2010. The limitations of melting on the reactivation of  
405 silicic mushes. *J. Volcanol. Geotherm. Res.* 195, 97–105.  
406 doi:10.1016/j.jvolgeores.2010.06.006

407 Huber, C., Bachmann, O., Manga, M., 2009. Homogenization processes in silicic magma  
408 chambers by stirring and mushification (latent heat buffering). *Earth Planet. Sci. Lett.* 283,  
409 38–47. doi:10.1016/j.epsl.2009.03.029

410 Ito, H., Spencer, C.J., Danišik, M., Hoiland, C.W., 2017. Magmatic tempo of Earth’s youngest  
411 exposed plutons as revealed by detrital zircon U-Pb geochronology. *Sci. Rep.* 7, 12457.  
412 doi:10.1038/s41598-017-12790-w

413 Johannes, W., Holtz, F., 1996. *Petrogenesis and Experimental Petrology of Granitic Rocks*.  
414 Springer-Verlag, Berlin, Heidelberg, New York.

415 Kataoka, K., Nagahashi, Y., Yoshikawa, S., 2001. An extremely large magnitude eruption close  
416 to the Plio-Pleistocene boundary: reconstruction of eruptive style and history of the  
417 Ebisutoge-Fukuda tephra, central Japan. *J. Volcanol. Geotherm. Res.* 107, 47–69.  
418 doi:10.1016/S0377-0273(00)00300-0

419 Kimura, J.-I., Nagahashi, Y., 2007. Origin of a voluminous iron-enriched high-K rhyolite magma  
420 erupted in the North Japan Alps at 1.75 Ma: Evidence for upper crustal melting. *J.*  
421 *Volcanol. Geotherm. Res.* 167, 81–99. doi:10.1016/j.jvolgeores.2007.02.004

422 Lange, R.A., 1994. The Effects of H<sub>2</sub>O, CO<sub>2</sub> and F on the Density and Viscosity of Silicate  
423 Melts. *Rev. Mineral. Geochemistry* 30, 331–370.

424 Lee, C.-T.A., Morton, D.M., Farner, M.J., Moitra, P., 2015. Field and model constraints on  
425 silicic melt segregation by compaction/hindered settling: The role of water and its effect on  
426 latent heat release. *Am. Mineral.* 100, 1762–1777.

427 Marsh, B.D., 1981. On the crystallinity, probability of occurrence, and rheology of lava and  
428 magma. *Contrib. to Mineral. Petrol.* 78, 85–98. doi:10.1007/BF00371146

429 McKenzie, D., 1984. The Generation and Compaction of Partially Molten Rock. *J. Petrol.* 25,  
430 713–765. doi:10.1093/petrology/25.3.713

431 Melekhova, E., Annen, C., Blundy, J., 2013. Compositional gaps in igneous rock suites  
432 controlled by magma system heat and water content. *Nat. Geosci.* 6, 385–390.  
433 doi:10.1038/ngeo1781

434 Pistone, M., Arzilli, F., Dobson, K.J., Cordonnier, B., Reusser, E., Ulmer, P., Marone, F.,  
435 Whittington, A.G., Mancini, L., Fife, J.L., Blundy, J.D., 2015. Gas-driven filter pressing in

436           magmas: Insights into in-situ melt segregation from crystal mushes. *Geology* 43, G36766.1.  
437           doi:10.1130/G36766.1

438 Pistone, M., Caricchi, L., Ulmer, P., Reusser, E., Ardia, P., 2013. Rheology of volatile-bearing  
439           crystal mushes: Mobilization vs. viscous death. *Chem. Geol.* 345, 16–39.  
440           doi:10.1016/j.chemgeo.2013.02.007

441 Rudnick, R.L., Gao, S., 2003. Composition of the Continental Crust, in: *Treatise on*  
442           *Geochemistry*. Elsevier, pp. 1–64. doi:10.1016/B0-08-043751-6/03016-4

443 Scaillet, B., Evans, B.W., 1999. The 15 June 1991 Eruption of Mount Pinatubo . I . Phase  
444           Equilibria and Pre-eruption P–T–*f*O<sub>2</sub>–*f*H<sub>2</sub>O Conditions of the Dacite Magma. *J. Petrol.* 40,  
445           381–411.

446 Vigneresse, J.-L., 2014. Textures and melt-crystal-gas interactions in granites. *Geosci. Front.*  
447           doi:10.1016/j.gsf.2014.12.004

448 Whitney, J.A., 1988. The origin of granite: The role and source of water in the evolution of  
449           granitic magmas. *Geol. Soc. Am. Bull.* 100, 1886–1897.

450 Wotzlaw, J., Bindeman, I.N., Watts, K.E., Schmitt, A.K., Caricchi, L., Schaltegger, U., 2014.  
451           Linking rapid magma reservoir assembly and eruption trigger mechanisms at evolved  
452           Yellowstone-type supervolcanoes. *Geology* 42, 807–810. doi:10.1130/G35979.1

453

454

455 **FIGURE CAPTIONS**

456 Figure 1:

457 Evidence of melt segregation in the upper section of the Takidani Pluton. Variations of Rb/Sr  
458 whole-rock content from GDT to pGT and QEMSCAN images with interstitial quartz (pink),  
459 orthoclase (green) and plagioclase with anorthite content <30wt.% (red). All other abundant  
460 mineral phases (including plagioclase phenocrysts) are represented in different shades of grey.  
461 Interstitial quartz, alkali feldspar and plagioclase (An<30) are considered to represent the  
462 residual melt of the magma, which gradually increases from the equigranular GDT unit towards  
463 the porphyritic pGT unit. The values below the bars show the content of quartz, orthoclase and  
464 albite, normalized to a fraction of 1. These values remain relative constant and suggest that the  
465 residual melt composition was buffered at the granitic minimum (Johannes and Holtz, 1996).

466

467 Figure 2:

468 Crystal fractionation trends from whole-rock and mineral analyses; (a) Assimilation and  
469 fractional crystallization (AFC) models (Hartung et al., 2017) performed on whole rock analyses  
470 show that compositional diversity is dominantly produced by crystal fractionation. The grey  
471 dashed lines and numbers on the side show the amount of melt (i.e. 60 wt.%) and assimilation  
472 (i.e. 3.2 wt.%). (b) Concentrations of Rb in plagioclase phenocrysts increase from 0.54 to 1.31  
473 ppm from core to rim, respectively, and point towards a progressive enrichment of the  
474 incompatible element Rb in the melt phase through crystal fractionation. The grey dashed lines  
475 and number below indicate the amount of melt fraction.

476

477 Figure 3:

478 Comparison between rhyolite-MELTS simulations (lines) and the matrix glass compositions  
479 (circles) measured between 950°C and 800°C by Costa et al. (2004). The color contouring  
480 indicates the initial water content of the starting material (Costa et al. 2004). Rhyolite-MELTS  
481 and experiments are in broad agreement and show the effect of initial water content on the  
482 chemical evolution of residual melt with decreasing temperature. No experimental data is  
483 available below 800°C.

484

485 Figure 4:

486 Results of rhyolite-MELTS simulations for dacitic magma. The colors show different initial  
487 water content of the magma, from 1 wt.% H<sub>2</sub>O (red line) to H<sub>2</sub>O saturated (black line). (a)  
488 Evolution of the residual melt water content as function of temperature. (b) Relationship between  
489 water content of the residual melt and melt fraction. (c) Silica content of the residual melt versus  
490 temperature. d) Water content versus silica content of the residual melt.

491

492 Figure 5:

493 Physical parameters of hydrous dacitic magma during melt evolution from rhyolite-MELTS  
494 simulations. (a) Temperature decreases with decreasing melt fraction. (b) Evolution of melt  
495 viscosity during magma crystallization of H<sub>2</sub>O-saturated and undersaturated dacitic magma. (c)  
496 The density difference between crystals and the residual melt is large near the liquidus  
497 temperature but becomes less pronounced towards lower melt fractions. (d) Relative time magma  
498 spends within each fraction interval based on enthalpy budget.

499

500 Figure 6:

501 Hindered settling velocities (Bachmann and Bergantz, 2004) of dacitic magma with different  
502 initial water content ( $H_2O_i$ ). Physical properties are obtained from rhyolite-MELTS simulations.  
503 Melt segregation is most effective for hindered settling at its maximum melt fractions of 0.5-0.6.  
504 Magmas with  $H_2O_i \geq 3$  wt.% segregate at the same rate below a melt fraction of 0.55. Magmas  
505 with lower initial water contents have velocities of up to one magnitude lower. All velocities are  
506 calculated for a fixed crystal size (i.e. radius) of 3 mm.

507

508 Figure 7:

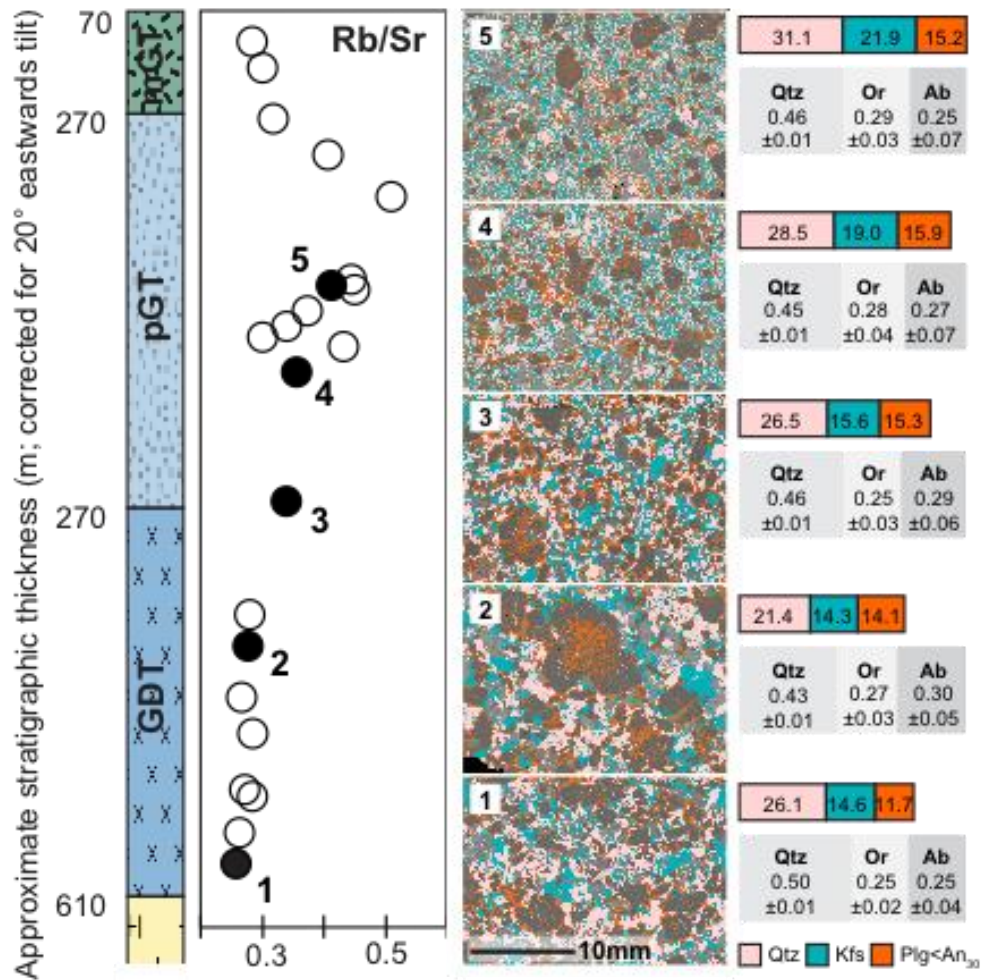
509 Simulations of residual melt extraction within rheologically locked window for different initial  
510 water contents, reservoir volumes (V) and thicknesses (Th). Each line represents one calculation  
511 and the cumulative distance travelled by the residual melt for a given reservoir thickness  
512 (numbers next to the colored lines).

513

514 Figure 8:

515 a) Regime diagram showing the regions of  $H_2O_i$  and thickness of the magma reservoir best suited  
516 for the formation of melt caps or lenses. For water content of 1 wt.% there is essentially no  
517 significant residual melt segregation before solidification. The dashed lines separate the field  
518 where melt caps (below or to the right of the line) and melt lenses (above or to the left of the  
519 line) for magmas with different  $H_2O_i$ . For higher  $H_2O_i$  the potential of forming melt caps  
520 increases with increasing reservoir volume. Grey zones indicate regions where melt lenses may  
521 form instead of melt caps.

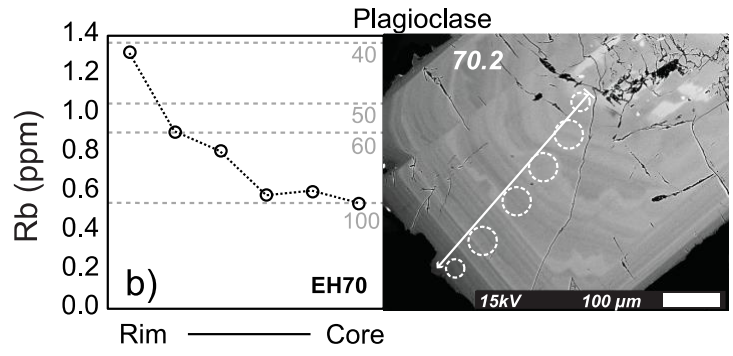
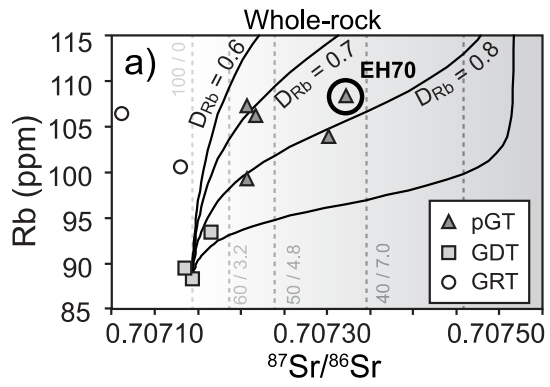
522



523

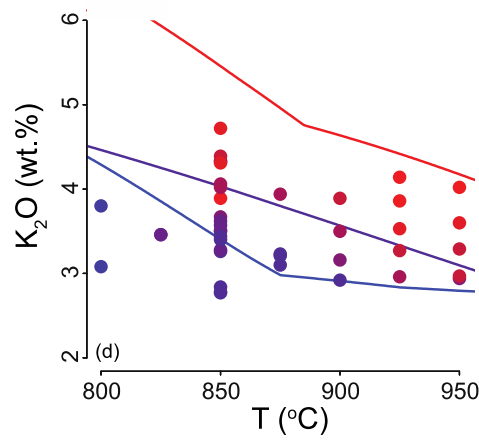
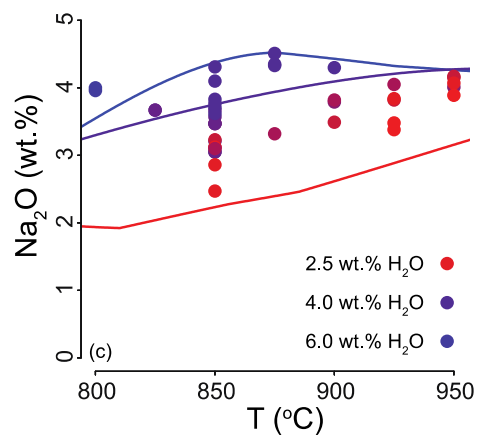
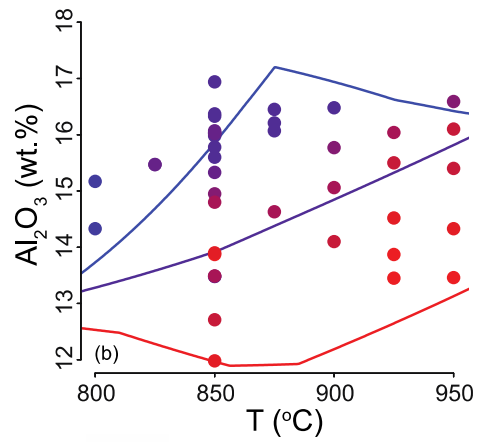
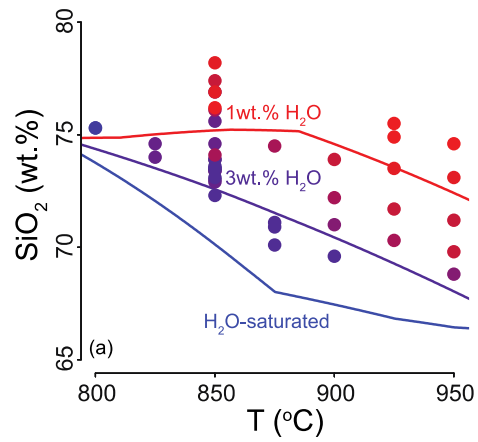
524





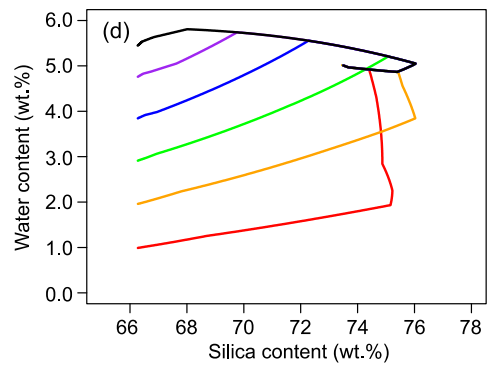
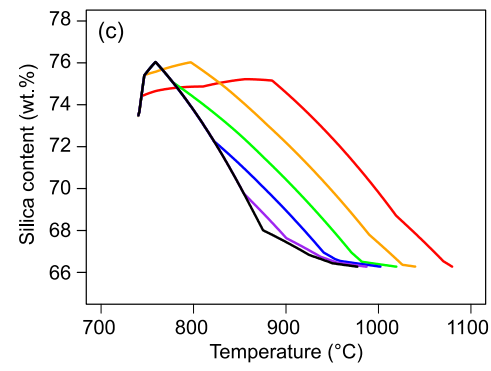
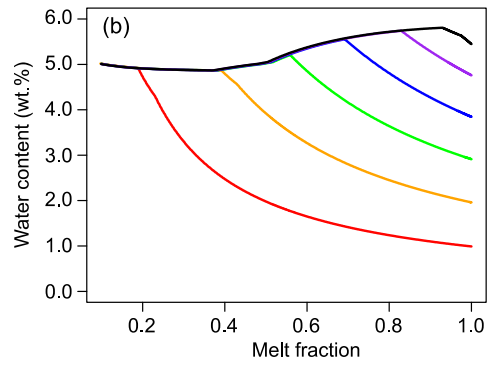
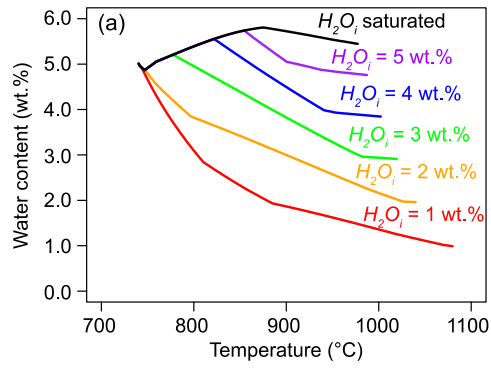
525

526



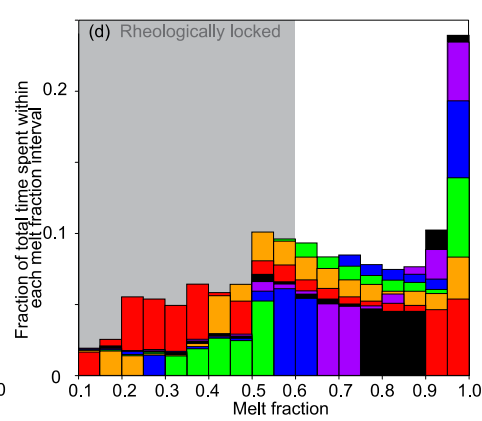
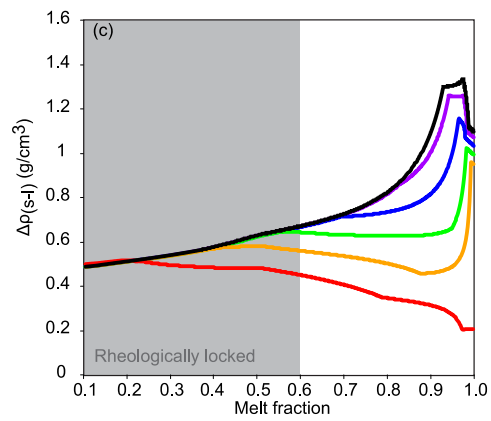
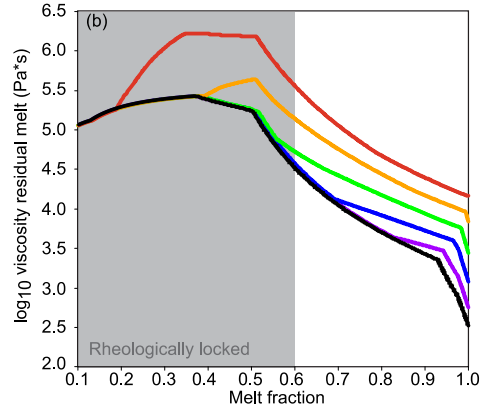
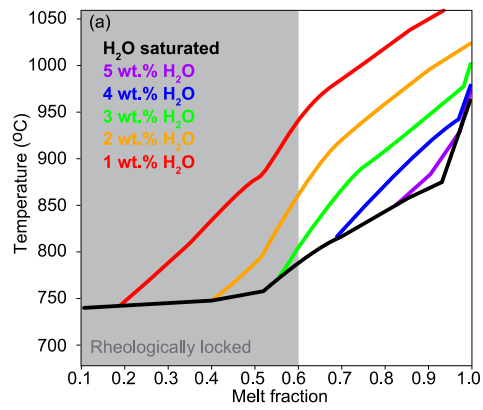
527

528



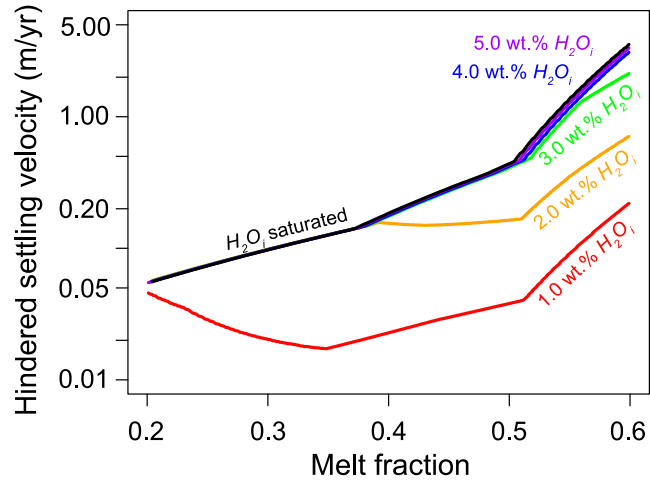
529

530



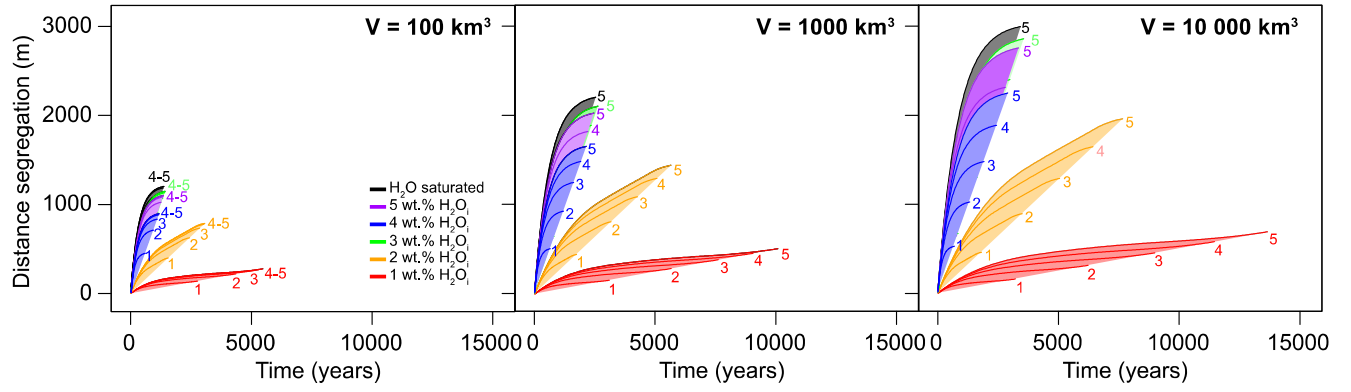
531

532



533

534



535

536

